LUND UNIVERSITY

Polarisation-resolved super-resolution microscopy

WOUTER DUVERGER

Polarisation-resolved super-resolution microscopy

by

Wouter Duverger

In partial fulfilment of the requirements for the degree of

MSc in Physics
Biological Physics and Computational Biology,

at the NanoLund Centre for Nanoscience, Lund University,
to be defended publicly on (May 20, 2021).

Project duration	4 months (full-time equivalent)
Supervision	prof. dr. Jonas Tegenfeldt
Daily supervision	dr. Jason Beech
Examiner	prof. dr. Edouard Berrocal

LUND UNIVERSITY

NANOLUND

NANOTECHNOLOGY FOR THE FUTURE

Contents

Abstract ii

Nomenclature iii

1 Introduction 1

2 Background 2
- 2.1 Diffraction-limited fluorescence microscopy . . . 2
- 2.2 Polarisation microscopy . . . 4
- 2.3 Super-resolution microscopy . . . 6

3 Methods 8
- 3.1 Microscope setup . . . 8
- 3.2 Data analysis of conventional polarisation images . . . 10
- 3.3 Polarisation-resolved STED microscopy (pSTED) . . . 10
- 3.4 Samples used in this thesis . . . 10

4 Results 11
- 4.1 Validating the laser modules . . . 11
- 4.2 Validating the detection module . . . 11
- 4.3 Demonstration of conventional polarisation microscopy . . . 12
- 4.4 Polarisation-resolved STED microscopy . . . 13

5 Outlook 15

A References 16

B Acknowledgements 18

C Code and data availability 19

D A note on laser safety 20

E Supplemental figures 22

Abstract

(to do)

Nomenclature

APD	Avalanche photodetector
AOM	Acousto-optical modulator
CCD	Charge-coupled device
GFP	Green fluorescent protein
HWP	Half-wave plate
MPE	Maximum permissible exposure
NA	Numerical aperture
OD	Optical density (an OD2 filter reduces the light intensity by a factor of 10^2)
PMT	Photomultiplier tube
PSF	Point spread function
pSTED	Polarisation-resolved stimulated emission depletion microscopy
QWP	Quarter-wave plate
SiR	Silicon-rhodamine
SLM	Spatial light modulator
STED	Stimulated emission depletion microscopy
TCSPC	Time-correlated single photon counter

1

Introduction

2

Background

(Why do we want to see small things?)

Microscopy - imaging structures at microscopic scales - is an extremely wide and varied field. It is widely accepted to have began in the sixteen-hundreds, with Antoni van Leeuwenhoek's discovery of bacteria and other single-celled organisms (ref). After that, microscopes have been getting higher resolution, but as lenses got better and better, they were not the resolution bottleneck any more. Specifically, in 1873, Ernst Abbe determined that the best possible focus that a microscope can reach is limited by the wavelength of the light used (ref). This meant that the microscopes of the time were limited to a resolution of roughly 400 nm (assuming focused visible white light). It was long believed that the Abbe limit was a fundamental limit of nature, and that the only way around it was by using light of a different wavelength. This is one of the reasons for the development of electron microscopes (ref), as quantum mechanics postulates that accelerated electrons have much shorter wavelength than visible light.

2.1. Diffraction-limited fluorescence microscopy

Fluorescence microscopy is an invaluable tool in modern biology [4]. Unlike other methods, it is able to tag specific protein species and other relevant molecules in the cell with a fluorescent label. There are thousands of small organic fluorescent labels, and more are being developed [15, 11]. The introduction of GFP and other fluorescent proteins was a remarkable development in the field, as labels can now be genetically fused to proteins of interest [12, 8]. There were over thirty thousand papers collected in the PubMed database that mentioned fluorescence in the year 2020 alone. I will first explain the physical phenomena behind fluorescence, and then discuss the limitations of this class of microscopy methods. (resolution, bleaching, ...)

Fluorescence. In short, fluorescence is a phenomenon in which a molecule absorps a photon of one wavelength, spends a short amount of time in an excited energy state, and then emits a photon of another (longer) wavelength. The difference in wavelength is essential to perform microscopy, and the fact that molecules have discrete energy states is key to get there.

Let us consider a molecule with two electronic energy states, each of which has a number of vibrational energy levels as in Figure 2.1. When the molecule is in its ground state (the lowest available energy level), it can absorb photons only if the energy they carry matches the difference between the ground state and another energy level. From an excited state, the system can relax into lower vibrational levels without emitting radiation, after which it emits a photon, relaxing back to the ground state. Two possible paths are shown in the figure. Because some energy is lost in a non-radiative way, the emitted photons will carry less energy than the absorbed photon, resulting in the wavelength difference mentioned before. This is also called the Stokes shift.

The precise energy levels available depend on the molecule and its environment. Therefore, every fluorescent molecule has a unique absorption and emission spectrum, which needs to be considered when planning a fluorescence experiment.

The diffraction limit. We'll consider the diffraction limit in one of the simplest possible setups: an epifluorescence microscope. Epifluorescence microscopy is fairly similar to bright field microscopy. The sample, which is stained with a fluorescent dye, is illuminated with a laser at a wavelength that dye

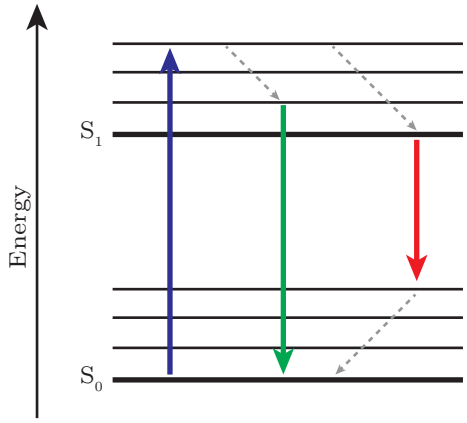

Figure 2.1: Illustration of the discrete energy states of a molecule and some possible transitions between them. The difference between energy levels determines the wavelength and colour of the absorbed or emitted photon.

Table 2.1: Some common definitions of the resolution limit d_{xy}.

Name	Criterion	Definition
Raileygh	The first minimum of one point's Airy function coincides with the maximum of another	$d_{xy} = .61\lambda/\mathrm{NA}$
FWHM	The width of the Airy function at half of the peak height	$d_{xy} = .51\lambda/\mathrm{NA}$
Abbe	(what did he base it on?)	$d_{xy} = .5\lambda/\mathrm{NA}$
Sparrow	The distance between fluorophores at which the brightness between two peaks is constant	$d_{xy} = .47\lambda/\mathrm{NA}$

can absorb. The dye molecules will then emit photons of longer wavelengths in their emission spectrum, which are collected by the microscope objective. Before imaging by a CCD camera, the scattered laser light can be filtered away using a dichroic mirror that passes emission light and reflects excitation light.

It used to be the case that microscopes were limited in resolution by the quality of their lenses and the pixel density of the CCD, but there is a much more fundamental limit, first described by Ernst Abbe. This limit is caused by the presence of an aperture. When a beam of light goes through an aperture of finite size, such as a lens, it cannot be focused onto an infinitesimal point. Instead, it will generate a spot with a radius approximately equal to $\lambda/2\mathrm{NA}$, where λ is the wavelength of the light and $\mathrm{NA} = n \sin\theta$ is the numerical aperture, the product of the index of refraction and the sine of the half-cone angle of the acceptance cone.

In particular, a circular aperture will convert point sources in the sample plane to Airy patterns in the image plane. Mathematically, this can be described by a convolution product between the point spread function (PSF) h and the object O,

$$I(\mathbf{x}) = (h * O)(\mathbf{x}) \coloneqq \int \mathrm{d}^3\mathbf{x}'\, h(\mathbf{x} - \mathbf{x}')O(\mathbf{x}'), \tag{2.1}$$

resulting in an image I. When two fluorophores are close enough together that their PSFs overlap, they appear as a single object instead of two separate ones. This happens when the distance between them is around $\lambda/2\mathrm{NA}$, and that is what determines the resolution of a microscope. The exact resolution depends on your definition of this minimum resolvable distance. There are several definitions, but they are all proportional to λ/NA. Some of them are listed in Table 2.1.

For a long time, physicists thought this limit was practically unavoidable [9], but in the next sections, I will discuss two ways in which one can get information from a system below the resolution limit. The first is indirect and requires playing with a new aspect of light (polarisation) that allows you to get information about structures that you cannot see. The second (STED microscopy) directly increases the image resolution. The excitation light is still subject to the Abbe limit, but we add another laser to effectively improve our focusing.

Table 2.2: List of a number of polarisation states.

Polarisation state	E_{0x}	E_{0y}	δ	Jones vector
Linear along x	1	0	any	$(1, 0)$
Linear along y	0	1	any	$(0, 1)$
Linear at 45°	1	1	0	$(1, 1)$
Circular (left-handed)	1	1	$\pi/4$	$(1, i)$
Circular (right-handed)	1	1	$-\pi/4$	$(1, -i)$

2.2. Polarisation microscopy

The wave nature of light might limit the resolution of a microscope, but it can also be exploited in our favour. Light polarisation can inform on the orientation of structures in a sample that are smaller than the diffraction limit. Among other things, this has been used to measure how the structure of DNA changes when it is subject to a strong stretching force, how integrin proteins respond to an applied force and measure the order of molecules embedded in the cell membrane, among others [2, 10, 13, 3]. In this section, I will first introduce the concept of light polarisation, then discuss how it can be used in a microscope, and finally mention some optical components that affect the light polarisation, which are crucial to conducting a polarisation microscopy experiment.

The polarisation ellipse. Remember that light is a transverse electromagnetic wave. This means that there are oscillations of the electric and magnetic fields along the path of a light ray, and that these oscillations are orthogonal to the propagation direction. In other words, if the light propagates along $\mathbf{k}$, the electric and magnetic fields $\mathbf{E}$ and $\mathbf{B}$ must satisfy $\mathbf{E} \cdot \mathbf{k} = \mathbf{B} \cdot \mathbf{k} = 0$. (The fields themselves are also orthogonal to each other, so we can neglect $\mathbf{B}$ without compromising our analysis.)

For the sake of simplicity, let's consider a ray propagating in the z direction. The electric field at any point in space and time can be written as

$$E_x(z, t) = E_{0x} \cos(kz - \omega t + \phi_x), \tag{2.2}$$
$$E_y(z, t) = E_{0y} \cos(kz - \omega t + \phi_y). \tag{2.3}$$

where $\mathbf{E}_0$ is the amplitude of the oscillation, k is the wavenumber (the length of $\mathbf{k}$), ω is the radial frequency and ϕ is an arbitrary phase. Note that the wavenumber and the frequency are related to each other through the speed of light c, since $\omega = kc$. Note that the x and y components can have a phase difference.

Letting $\delta = \phi_y - \phi_x$, it can be shown that

$$\left(\frac{E_x}{E_{0x}}\right)^2 - 2\cos\delta \frac{E_x}{E_{0x}} \frac{E_y}{E_{0y}} + \left(\frac{E_y}{E_{0y}}\right)^2 = \sin^2\delta. \tag{2.4}$$

This is the equation for an ellipse. That means that, at any point in time, the point (E_x, E_y) lies on the ellipse defined by the equation above, which is called the polarisation ellipse. The ellipse is characterised by E_{0x}, E_{0y} and δ:

- if $E_{0x} = 0$, the ray is said to be linearly polarised in the y direction, and vice versa,
- if neither are equal to 0, but they are in phase (meaning $\delta = 0$), the light is still polarised, at an angle $\psi = \arctan(E_{0y}/E_{0x})$ to the x axis,
- if the amplitudes in x and y are equal, and $\delta = \pm\pi/4$, then the light is circularly polarised. If *delta* is positive (negative), the polarisation is said to be right-handed (left-handed). (replace this list by table)

In general, the polarisation ellipse can be defined by means of two angles: the orientation ψ and ellipticity χ, as shown in (figure of pol ellipse from field guide to polarisation). They can be calculated from $\alpha = \arctan(E_{0y}/E_{0x})$ and the phase difference δ using

$$\tan 2\psi = \tan 2\alpha \cos\delta, \tag{2.5}$$
$$\sin 2\chi = \sin 2\alpha \sin\delta. \tag{2.6}$$

Microscopy. Why is this relevant to microscopy? Well, since a fluorophore can be considered a small dipole moment, the absorption of excitation light that is linearly polarised along an angle ψ will depend on the dipole orientation θ. The intensity of light emitted by that fluorophore will then satisfy

$$I(\psi, \theta) \propto \cos^2(\psi - \theta). \tag{2.7}$$

This is Malus's law. Analogously, light emitted from a fluorophore is always linearly polarised parallel to its dipole. One can place a linearly polarising filter in front of the detector to measure a fluorophore's orientation. If the polariser emits light polarised at an angle ψ, then the intensity measured at the detector also follows Malus's law, meaning that these two setups are analogous (not taking into account depolarisation effects in an experimental setup). As an example, see (figure of sir actin from spira2017).

Jones calculus. To finish this section, I'd like to introduce Jones calculus. This is an incredibly useful way to model light polarisation, as well as how it interacts with certain optical components that are present in our system, but it does require us to express the the electric field with a complex function. Let us express it as follows:

$$\mathbf{E}(z, t) = \mathbf{E}_0 e^{i(kz - \omega t)}. \tag{2.8}$$

In the following analysis, we will treat $\mathbf{E}$ as a two-dimensional vector with only an x and y component, as $E_z = 0$. Note that complex numbers are just a mathematical trick. The Maxwell equations that govern light propagation are linear, and taking the real part of a complex-valued function is also a linear operation, so the complex extension of $\mathbf{E}$ will behave exactly the same as the actual electric field would. The phase difference between the two components is now contained in $\mathbf{E}_0$, which looks like

$$\mathbf{E}_0 = \begin{pmatrix} E_{0x} \\ E_{0y} e^{i\delta} \end{pmatrix}. \tag{2.9}$$

The Jones vectors for some special polarisation states are listed in Table 2.2.

The usefulness of Jones calculus lies in its ability to represent optical components as matrices acting on this vector. For example, a polariser that transmits x-polarised light has the following matrix form:

$$S_p = \begin{pmatrix} 1 & 0 \\ 0 & 0 \end{pmatrix}. \tag{2.10}$$

It is easy to verify that $S_p \mathbf{E}_0 = E_{0x}$. (ref further along with rotated components to prove malus' law) We also need to take into account how mirrors affect polarisation. A mirror flips the field component that is orthogonal (the s-component) to the mirror surface, while keeping the other component (p) unchanged. So, a mirror whose surface is parallel to the x-axis has a Jones matrix of the form

$$S_{mx} = \begin{pmatrix} 1 & 0 \\ 0 & -1 \end{pmatrix}. \tag{2.11}$$

Another important type of optical component in our setup is a waveplate. Waveplates or phase retarders are birefringent crystals, meaning the index of refraction a ray of light experiences is dependent on its polarisation. This happens when a crystal structure is not symmetric. (what kind of symmetry?) In these crystals, Equation 2.8 is no longer valid and should be substituted by

$$\mathbf{E}(z, t) = \begin{pmatrix} E_{0x} e^{i(k_x z - \omega t)} \\ E_{0y} e^{i(k_y z - \omega t + \delta)} \end{pmatrix}, \tag{2.12}$$

assuming the optical axes of the waveplate are along x and y. This can also be written as

$$\mathbf{E}(z, t) = \begin{pmatrix} E_{0x} \\ E_{0y} e^{i(\Gamma(z) + \delta)} \end{pmatrix} e^{i(k_x z - \omega t)} \quad \text{, where} \quad \Gamma(z) = (k_y - k_x) z. \tag{2.13}$$

As one can see, a waveplate only imparts a delay on the y-component of a beam, depending on its thickness z and its birefringence. We can neglect the common phase factor and represent the action of a waveplate by the following Jones matrix,

$$S_\Gamma = \begin{pmatrix} 1 & 0 \\ 0 & e^{i\Gamma} \end{pmatrix}. \tag{2.14}$$

Generally, waveplates are characterised by the relative delay they impart on the slowly propagating polarisation component. Quarter-wave plates delay it by a quarter of a wavelength compared to the fast propagating ray, corresponding to $\Gamma = \pi/2 + 2n\pi$ (for any integer n). Therefore, the Jones matrix of a quarter-wave plate satisfies

$$S_{\lambda/4} = \begin{pmatrix} 1 & 0 \\ 0 & i \end{pmatrix}. \tag{2.15}$$

Let's consider what happens to some specific cases. If vertically or horizontally polarised light passes through a quarter-wave plate, its polarisation will not change. But light polarised along $+45°$ ($-45°$) will be turned into left-handed (right-handed) light, and vice versa. Therefore, a quarter-wave plate allows us to convert between linearly and circularly polarised light. (figure of waveplate actions)

The second type of waveplate we should treat is a half-wave plate. It features a delay of $\Gamma = \pi + 2n\pi$, and its Jones matrix looks like

$$S_{\lambda/2} = \begin{pmatrix} 1 & 0 \\ 0 & -1 \end{pmatrix}, \tag{2.16}$$

which corresponds to mirroring the polarisation state along the x-axis. Another way to think about that is that a ray polarised along an angle ψ will be rotated by an angle -2ψ. Circularly polarised light will get the opposite handedness.

As said before, the power of Jones calculus lies in its ability to model the behaviour of a sequence of optical elements at arbitrary rotations. First, we need to define the Jones matrix for a rotated component. This is simply

$$S(\theta) = R(\theta) \cdot S \cdot R(-\theta) \quad \text{, where} \quad R(\theta) = \begin{pmatrix} \cos\theta & -\sin\theta \\ \sin\theta & \cos\theta \end{pmatrix} \quad \text{(check!)} \tag{2.17}$$

and θ is the angle of the component's x'-axis with the lab coordinate system's x-axis. (introduce). As an example, let's recover Malus's law by sending linearly polarised light through a half-waveplate at an angle $\theta/2$ (such that the light is polarised along θ after it) and then through a polariser.

$$I(\theta) \propto \left| S_p(0) \cdot S_{\lambda/2}(\theta/2) \cdot \begin{pmatrix} 1 \\ 0 \end{pmatrix} \right|^2 = \cos^2\theta. \tag{2.18}$$

To do

- Moeller calc
- Hinting at psted

2.3. Super-resolution microscopy

There are several ways to glean information below the resolution limit. Some use optical properties of the sample to their advantage, like light polarisation or fluorescence resonance energy transfer (FRET) [7], others use the photophysics of individual dyes to turn off a subset of them during imaging. On the one hand, there are stochastic methods like STORM and PALM. On the other, there are targeted techniques such as STED, GSD, RESOLFT, ... (explain acronyms) The Tegenfeldt group own a STED microscope. I will use this section to explain STED microscopy.

In essence, a STED microscope is a confocal microscope with an added laser that can selectively deplete fluorescence by stimulated emission.(schematic of a sted microscope) In a confocal microscope, the excitation laser does not illuminate the whole sample at once, but is scanned over it. This means only fluorophores in an Airy disk around the focus will be excited. Furthermore, the detector is now comprised of a pinhole and a photodetector (not a camera), which filters out most of the out-of-focus light. Therefore, the PSF of a confocal microscope is the product of the laser PSF h_{exc} and the detection probability h_{det}

$$h_{conf}(\mathbf{x}) = h_{exc}(\mathbf{x}) \cdot h_{det}(\mathbf{x}). \tag{2.19}$$

Even though both of these PSFs are diffraction-limited, a STED microscope can reach an arbitrarily small resolution [14]. It does so by illuminating the sample with a donut-shaped laser at a wavelength longer than the emission wavelength. Referring back to Figure 2.1, the blue laser excites the fluorophores that emit in green, but a red transition is also allowed. Under illumination with a red laser, this transition is made more favourable by the process of stimulated emission, first postulated by Einstein in 1926 [5]. This way, fluorophores at the edge of the excitation PSF can be prevented from emitting green light,

while fluorophores at the centre do not experience stimulated emission, which reduces the width of the effective point spread function. An illustration of this effect is given in (figure).

(how to generate the donut? or in methods?)

Of course, the extent of the resolution improvement depends on the intensity of the depletion laser I_{dep}. The STED resolution is

$$d_{STED} = \frac{d_c}{\sqrt{1 + d_c^2 a^2 \frac{I_{dep}}{I_{sat}}}}, \tag{2.20}$$

where d_c is the resolution limit of a confocal microscope, a the steepness of the donut pattern, and I_{sat} is the depletion intensity at which fluorophore brightness is reduced by half [6].

3

Methods

3.1. Microscope setup

The Tegenfeldt microscope is a confocal fluorescence microscope constructed by Abberior Instruments GmbH (Germany). It features two excitation lasers (at 561 nm and 640 nm) and one depletion laser at 775 nm for two-channel confocal or STED microscopy. It also contains a time-correlated single photon counter (TCSPC) for fluorescence lifetime imaging microscopy (FLIM) and a highly sensitive photomultiplier tube (PMT). Refer to Figure 3.1 for the layout of these optical elements. Samples are located inside an inverted Nikon microscope body (Ti-E, not shown in the figure) equipped with a piezo stage (M-687 PILine XY-stage system and P-736 PInano (Physik Instrumente) Z Microscope Scanner), a 60x, 1.4 NA oil immersion objective (Nikon Plan Apo) and a QUADScan beam scanner (Cambridge Technology).

In this section, I will address all laser lines as well as the detection module in detail, with a focus on characterising the light polarisation at different points in the microscope.

The excitation lasers. This fast-switching 561 nm laser is initially horizontally polarised, but the polarisation can be tuned by three waveplates in its path. The last one, a quarter-wave plate, is fixed in its rotation angle. In the standard mode of operation, excitation laser light should be circularly polarised to minimise resolution reduction due to lens distortion etc. [6]. In that mode, the (fast or slow) axis of the first quarter-wave plate should be aligned with the laser, such that it does not affect polarisation and the half-wave plate should be set such that it rotates the (linearly polarised) light to 45° with respect to the second quarter-wave plate. See (table) for the polarisation characteristics in the calibration provided by Abberior. (mention in words that it's very good)

The 640 nm laser does not have fast-switching built in, so instead the light is fed into the microscope through a polarisation-polarisation optical fibre by an acousto-optical modulator (AOM). The AOM is a crystal in the beam path, in which sound waves can be generated by a piezo element. The ray is deflected by an angle that depends on the frequency of these waves, such that the laser beam can quickly be aligned into or away from the fibre aperture. The rest of the beam path is very similar to the 561 module, but the calibration of the waveplates in this pathway are not as accurate. Refer to (table).

The STED module. The depletion laser travels through an entirely different set of optics than the excitation lasers to generate a donut beam. First, it travels through a half-wave plate that aligns the polarisation to the SLM (spatial light modulator). The SLM adds an arbitrary spatially patterned phase delay to the light falling on it, but only if light is polarised along its active axis. It will not alter the phase of the orthogonally polarised component. Using the proper phase delay patterns, one can create any (diffraction-limited) image in the sample plane. In our case, that would be a donut shape. Then – and I am ignoring the pSTED module for now – the light travels through a half-wave plate to ensure circular polarisation in the sample plane, just like the excitation lasers. This is done to ensure that the depletion efficiency does not depend on sample orientation and to avoid polarisation-dependent PSF distortion by lenses and other optics.

The detection module. The main detectors of the microscope are a set of avalanche photodiodes (APDs), but there is also a highly sensitive photomultiplier tube (PMT) right after the QWP on the microscope end. The PMT is usually used to measure the point spread functions of the lasers and to

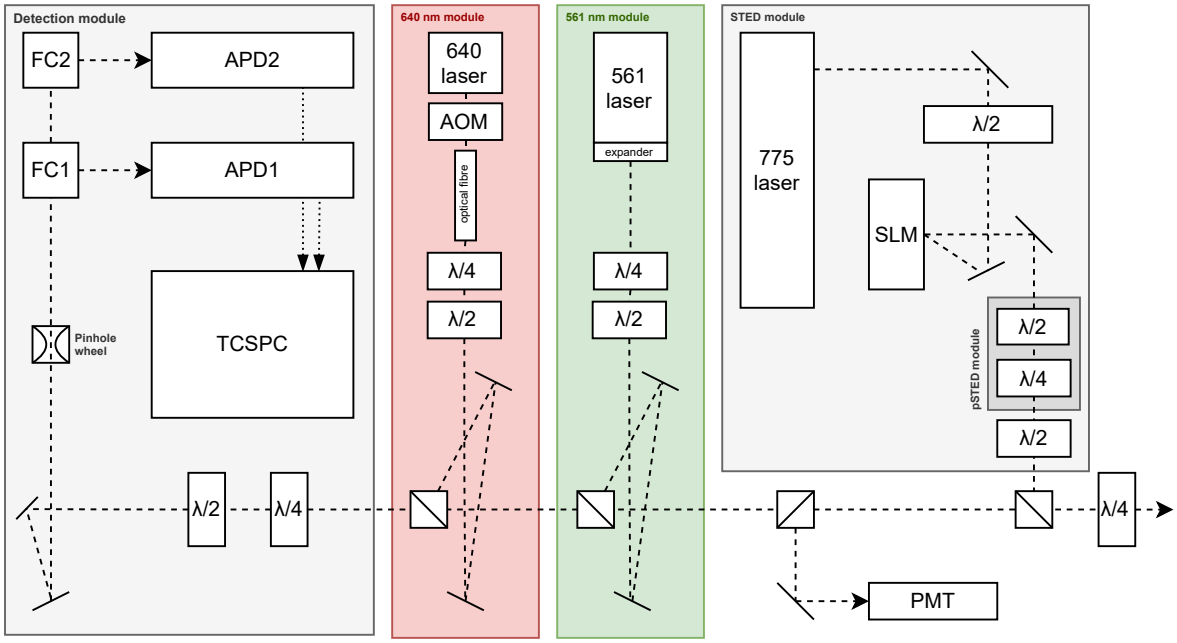

Figure 3.1: Schematic overview of the Tegenfeldt microscope. The sample is located in a microscope housing on the bottom right (outside this figure). FC1 and FC2 are filter cube housings. Half-wave and quarter-wave plates are denoted $\lambda/2$ and $\lambda/4$, respectively. Dashed lines represent the light path, except those that go to the TCSPC (those are digital connections). The waveplates in the pSTED module were not in the original setup, and were added by us. See text for more details.

align them. In normal operation, the light travels on to the detection waveplates, then through a pinhole wheel, passes filters and dichroics in the filter cube housings, and is finally reflected onto the APDs. The wheel contains pinholes of different sizes, which allows for choosing the trade-off between light collection and z resolution. Different filter cubes are available with various notch filters, dichroic mirrors, and/or a polarising beam splitter (PBS).

The APDs show a slight polarisation sensitivity, of about 10% of the maximum sensitivity (see Figure E.5). I measured this by exciting Tetraspec beads with the 561 laser set to circular excitation, such that the emission light is non-polarised. Then I put a linear polariser on (This actually seems to be on the order of the 561 circularity error! Analyse that data.)

We did have some problems with the waveplates in the detection module. They can be controlled through Abberior's software suite (Imspector), but it is not clear if they are set up correctly. The calibration is based on a control angle that I will call θ. It would be possible for this setup to rotate polarised light of any orientation, since

$$S_{\lambda/2}(\theta/2)S_{\lambda/4}(0)S_{\lambda/4}(0) = \begin{pmatrix} \cos\theta & -\sin\theta \\ \sin\theta & \cos\theta \end{pmatrix}, \tag{3.1}$$

which is simply the rotation matrix $R(\theta)$. The exact position of the quarter-wave plates does not matter, but it is important that they are aligned with each other. If the waveplates are at a different angle ϕ, then this set of waveplates rotates the polarisation by an angle $(\theta - 2\phi)$ instead. It is worth noting that the calibration provided by Abberior does something completely different, that we don't yet understand, so I developed a new calibration.

First, I had to figure what angle to set the second quarter-wave plate to in order to align it to the first one. I did this by placing a polariser in the sample holder (P1) and illuminating it with the top lamp, such that the light incident on the first quarter-wave plate was linearly polarised. Then I placed another polariser (P2) after the waveplates that I rotated to assess the linearity of the polarisation there. Aligning the quarter-waveplates with each other simply involved maximising the linearity.

Second, I assessed both Abberior's and my calibration. As presented in Figure 3.2, my calibration works really well. (Mention the problem and how we might fix it.)

(Mention the pol cube results.)

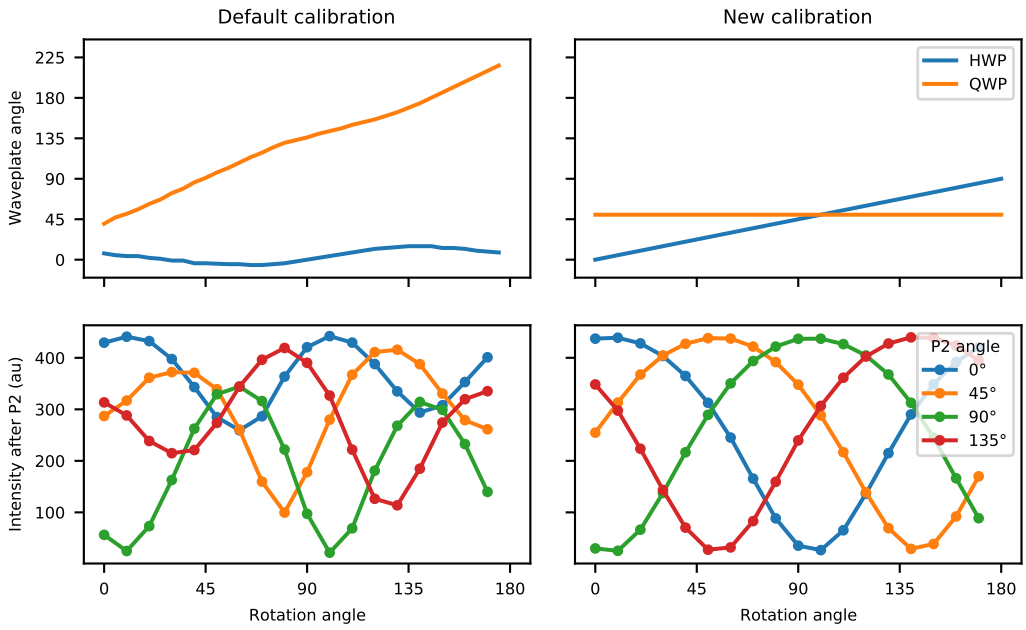

Figure 3.2: (text)

3.2. Data analysis of conventional polarisation images

3.3. Polarisation-resolved STED microscopy (pSTED)

3.4. Samples used in this thesis

4

Results

4.1. Validating the laser modules

For every laser in the setup (561 nm, 640 nm, and 775 nm), I measured the polarisation state of the light at different points in the beam path and at the sample plane, by measuring the power transmitted by a linearly polarising filter at different angles relative to the beam. At the sample location, the 640 nm beam is quite well-polarised when set to a linear polarisation. When rotating a polariser, the transmitted power drops to about one fifth of the maximum. At the circular setting, though, the light is quite elliptical, with a minimum power transmitted through the polariser being about half as bright as the maximum, see Figure E.1. The quality of the 561 nm polarisation is higher. When set to a linear polarisation, the power transmitted through a polariser drop from about 25 µW to a value almost equal to background levels around 0.1 µW, while the amplitude variations of the circularly polarised light are withing 14% of the mean, see Figure E.2. In conventional STED, the depletion beam is circularly polarised in order to achieve polarisation-independent quenching, so I also measured its polarisation state, see Figure E.3. The minimum power transmitted is about 63% of the max. (Calculate ellipticity angle, or introduce the E_{max}/E_{min} characteristic in the beginning.) (Put this stuff into a table?) (The fact that Emax/Emin is not amazing can be explained by depolarising effects of elements in the beam path)

There are two other things we can take away from those figures: the power of the 640 nm laser is not very constant. This can be explained by a slow ramp up to the set power every time the laser is turned on. Secondly, the noise on the signal from the 640 laser is higher. I believe this is due to the same effect. Therefore, I also measured the power profiles of the different lasers, see (figure). The conclusion from those measurements is that the response of the lasers to the desired power set in software is not linear at low powers. If experiments need to be done at low power, a neutral density filter is required. This is luckily not the case for biological specimens with a low density of fluorophores.

Finally, we also measured the PSFs of the different lasers as a sanity check. This is shown in Figure E.4. This data looks good. (Why does it look good?) (Mention how we got this data: PMT and gold beads.)

4.2. Validating the detection module

First off, I checked the polarisation dependence of the APDs. To do so, I ensured the light coming into the APDs was unpolarised by illuminating a sample of TetraSpec beads with circularly polarised 561 nm light, since that was the closest to circular that we could get. Then I put a polarising filter after the detection waveplates and measured the signal from the APD as a function of the incoming polarisation, see Figure E.5. For both APDs, there is a difference of about 4%.

To do:

- Should I do min/max like before? That would also be closer to a G factor, I guess.
- APD2 and power meter pol sensitivity.
- Correct for ellipticity of 561 polarisation

Second, I tested the effect of the detection waveplates on the polarisation state of incoming light. Linearly polarised input light was achieved by putting a polariser (P1) in the sample location and illuminating it with the microscope's top lamp. Then the intensity was measured by the APDs, which was dependent on the angle of a polariser located after the last waveplate (P2). Using Jones calculus, we

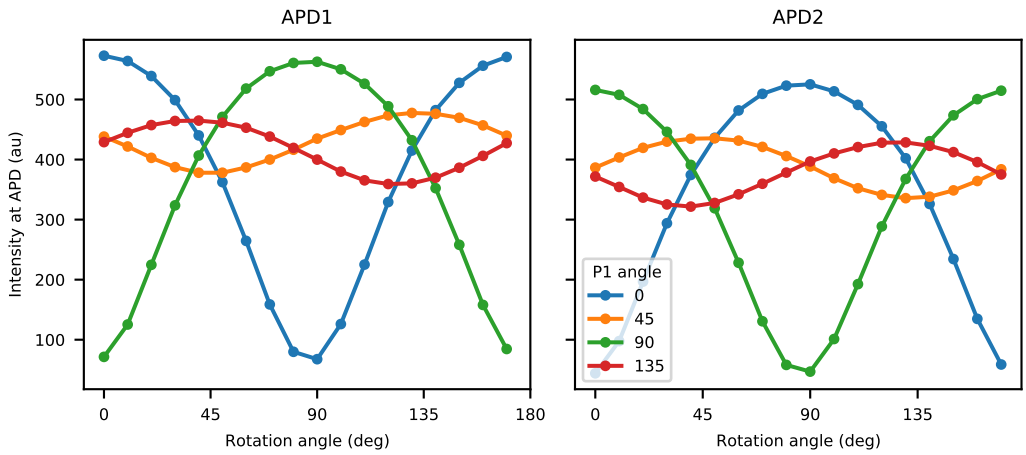

Figure 4.1: The POL cube distorts the polarisation state of incoming light. APD should measure the vertical component of the light (reflected by the POL cube), and APD2 should measure the horizontal component (transmitted). The detection waveplates were used to rotate incoming light, which was polarised along an angle shown in the legend.

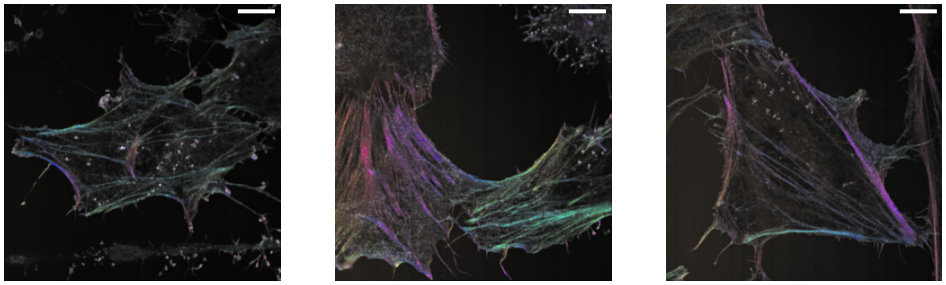

Figure 4.2: Polarisation microscopy images of three different cells. Scale bars 10 μm.

know that two QWPs and a HWP can form a proper polarisation rotator (ref methods), but the default calibration (a function that maps the total rotation angle to the angles the waveplates have to take on) is unable to do so. I determined that a better calibration sets the (non-fixed) QWP to an angle of 50° and the HWP to half the rotation angle. The angle of the QWP was chosen such that it is aligned with the fixed QWP at the microscope end. The behaviour of both calibrations is shown in Figure 3.2. The new calibration works as expected.

Finally, I also measured the polarisation characteristics of the POL cube. I generated linearly polarised light as in the previous paragraph, but left out P2. Then I rotated the polarisation using the detection waveplates and measured the intensity of light reflected and transmitted by the POL cube into APD1 and APD2 respectively. Apparently, the degree to which the POL cube can split the signal is strongly dependent on the polarisation of the light at the sample (the angle of P1), Figure 4.1. The cause of this effect is not immediately obvious, but is most likely due to some birefringence present in the POL cube. (Is that true?)

4.3. Demonstration of conventional polarisation microscopy

See Figure 4.2. To do:

- Colour wheels in the images
- sSTED + polarisation
- Can I get some quantitative results? (e.g. histograms of orientation/degree of polarisation, weighted by intensity)

4.4. Polarisation-resolved STED microscopy

(Refer back to the setup described in Methods.) The first step is to manipulate the polarisation of the depletion beam. Then I can do experiments on unpolarised and polarised controls (beads and Yersinia samples).

To get control of the light polarisation, the first step was to mount the new waveplates in the beam path. They were mounted after the SLM. The HWP was mounted inside a rotational stage and the QWP went in a cage system attached to the rotational stage, such that it is always aligned with the HWP, but its rotational angle is fixed. The first step was to find the angle of the QWP that maximised the linearity of the light polarisation at the sample. This was simply done by placing a polariser and a power meter at the sample and rotating them to characterise the polarisation of the depletion beam. I did this a couple of times, from which we concluded that the optimal angle for the QWP was 15°. (Does this warrant a figure? I'm not sure it's necessary.) Next, I had to find the angle of the HWP at which the depletion beam is vertically polarised. In that position, the depletion beam has a polarisation parallel to the excitation lasers (at 0°). This turned out to be 38.4°. See Figure E.6.

Now that we have control over the beam polarisation, we can check how the added waveplates influence the PSF. In (figure), the PSF is shown for different polarisation directions. There are a number of conclusions we can draw from this data. Firstly, the PSF is not circular any more, even though the SLM was set to Gaussian mode. In particular, the ellipse orientation is parallel to the light polarisation, so we see the PSF rotating in sync with the light polarisation. This can be explained by the fact that a lens interacts differently with light polarised along different directions. This is why we would usually use circularly polarised light instead.

Other effects of the polarisation include the following: the intensity of the depletion beam varies as a function of the polarisation angle. This is probably due to linear dichroism present in the optical elements between the waveplates and the sample. That is to be expected, but should be accounted during either image acquisition or analysis. Furthermore, the eccentricity of the ellipse has a slight dependency on the polarisation angle, and the maximum of the PSF moves a little: up to (?) nm from its mean position. Fortunately this is a quite a bit below the diffraction limit for 775 nm light, i.e. around 400 nm.

Fixed, non-polarised beads are a good control sample, since we can determine the polarisation of emitted light by selectively activating fluorophores of a particular orientation with the polarisation of the excitation light. That is called photoselection. (Remove this phrase if I discuss photoselection in Background.) When these beads are excited with circularly polarised light, fluorophores of all orientations should be activated equally, and the polarisation of the depletion beam should not matter. In the case of linearly polarised excitation light, on the other hand, depletion should be more efficient when its polarisation is aligned with the excitation beam. This can be verified by increasing the depletion power: when the beams are aligned, then the remaining fluorescence signal should drop faster than when they are not, as predicted by (ref equation from Background). Figure 4.3 shows that this is indeed the case. While there is some variation in the depletion rate under circular excitation, it can not be explained by the theory and seems random, unlike the case of linear excitation. There, depletion goes fastest when the beams are aligned, slower when there is a 45° angle between them, and slowest when they are orthogonal. If the depletion beam was even more linearly polarised (instead of Emin/Emax=.2), then this effect would be even more pronounced.

(pSTED results in cells.)

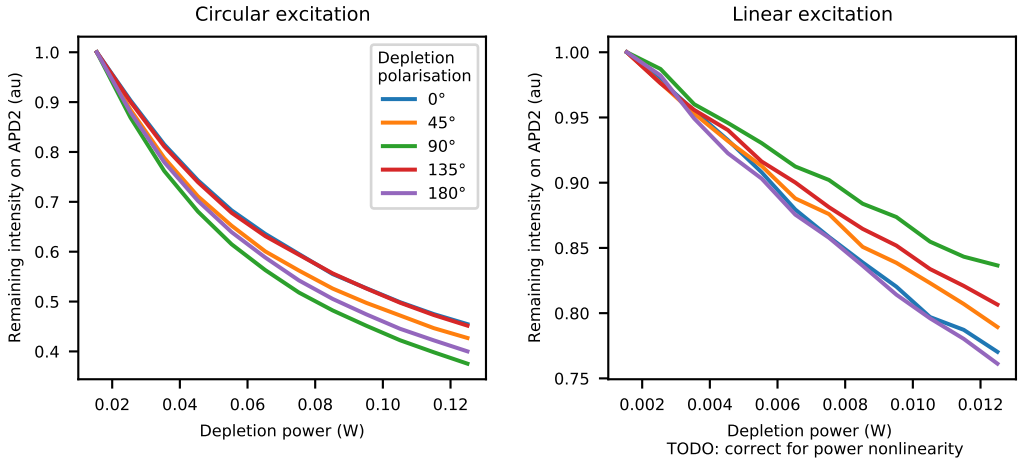

Figure 4.3: Dependency of surviving fluorescence on intensity and polarisation of depletion beam. **Left:** circular excitation. **Right:** linear excitation at 0° (vertical). (Maybe I should do a couple of repeats here, to make the figures more clear.)

5

Outlook

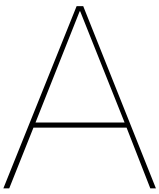

References

[1] Arbetsmiljöverket. *Artificiell optisk strålning, Arbetsmiljöverkets föreskrifter om artificiell optisk strålning och allmänna råd om tillämpningen av föreskrifterna*. https://www.av.se/globalassets/filer/publikationer/foreskrifter/artificiell-optisk-stralning-foreskrifter-afs2009-7.pdf. Accessed: 2021-03-15. 2019.

[2] Adam S. Backer et al. "Single-molecule polarization microscopy of DNA intercalators sheds light on the structure of S-DNA". In: *Science Advances* 5.3 (2019). ISSN: 23752548. DOI: 10.1126/sciadv.aav1083.

[3] Sophie Brasselet et al. "Imaging Molecular Order in Cell Membranes by Polarization-Resolved Fluorescence Microscopy". In: *Fluorescent Methods to Study Biological Membranes*. Berlin, Heidelberg: Springer Berlin Heidelberg, 2013, pp. 311–337. ISBN: 978-3-642-33128-2. DOI: 10.1007/4243_2012_51. URL: https://doi.org/10.1007/4243_2012_51.

[4] John SH Danial, Yasmine Aguib, and Magdi H Yacoub. "Advanced fluorescence microscopy techniques for the life sciences". In: *Global Cardiology Science and Practice* 2016.2 (2016). ISSN: 2305-7823. DOI: 10.21542/gcsp.2016.16.

[5] Albert Einstein. "Zur Quantentheorie der Strahlung". In: *Zeitschrift für Physik* 35.5 (1926), pp. 317–322. ISSN: 14346001. DOI: 10.1007/BF01380146.

[6] Benjamin Harke et al. "Resolution scaling in STED microscopy". In: *Optics Express* 16.6 (2008), p. 4154. ISSN: 1094-4087. DOI: 10.1364/oe.16.004154.

[7] Eitan Lerner et al. *FRET-based dynamic structural biology: Challenges, perspectives and an appeal for open-science practices*. 2021. DOI: 10.7554/eLife.60416.

[8] Mikhail E. Matlashov et al. "A set of monomeric near-infrared fluorescent proteins for multicolor imaging across scales". In: *Nature Communications* 11.1 (2020), pp. 1–12. ISSN: 20411723. DOI: 10.1038/s41467-019-13897-6. URL: http://dx.doi.org/10.1038/s41467-019-13897-6.

[9] C. W. McCutchen. "Superresolution in microscopy and the Abbe resolution limit." In: *Journal of the Optical Society of America* 57.10 (1967), pp. 1190–1192. ISSN: 00303941. DOI: 10.1364/JOSA.57.001190.

[10] Pontus Nordenfelt et al. "Direction of actin flow dictates integrin LFA-1 orientation during leukocyte migration". In: *Nature Communications* 8.1 (2017). ISSN: 20411723. DOI: 10.1038/s41467-017-01848-y. URL: http://dx.doi.org/10.1038/s41467-017-01848-y.

[11] Ute Resch-Genger et al. "Quantum dots versus organic dyes as fluorescent labels". In: *Nature Methods* 5.9 (2008), pp. 763–775. ISSN: 15487091. DOI: 10.1038/nmeth.1248.

[12] Nathan C. Shaner, Paul A. Steinbach, and Roger Y. Tsien. "A guide to choosing fluorescent proteins". In: *Nature Methods* 2.12 (2005), pp. 905–909. ISSN: 15487091. DOI: 10.1038/nmeth819.

[13] Vinay Swaminathan et al. "Actin retrograde flow actively aligns and orients ligand-engaged integrins in focal adhesions". In: *Proceedings of the National Academy of Sciences of the United States of America* 114.40 (2017), pp. 10648–10653. ISSN: 10916490. DOI: 10.1073/pnas.1701136114.

[14] Dominik Wildanger et al. "Solid immersion facilitates fluorescence microscopy with nanometer resolution and sub-Ångström emitter localization". In: *Advanced Materials* 24.44 (2012), pp. 309–313. ISSN: 09359648. DOI: 10.1002/adma.201203033.

[15] Jin Zhang et al. “Creating new fluorescent probes for cell biology”. In: *Nature Reviews Molecular Cell Biology* 3.12 (2002), pp. 906–918. ISSN: 14710072. DOI: 10.1038/nrm976.

(Improve bibstyle)

B

Acknowledgements

C

Code and data availability

D

A note on laser safety

The 775 nm line is a class 4 laser source. Under normal operation, the user is protected from it. However, when calibrating the STED beam or placing new components in the beam path, it is theoretically possible for the collimated laser beam to be reflected into the user's eyes. A high-powered laser beam can do permanent damage to the skin and retina, so we have to make sure we stay below the limits imposed by the Work Environment Agency's (Arbetsmiljöverkets) limits [1]. These regulations set forth three main conditions to calculate the Maximum Permissible Exposure (MPE) of a pulsed laser, see table 2.6 of the regulations. Important values and formulas about our setup, as well as the limits provided by the Work Environment Agency are provided in Table D.1 and in the text below.

Table D.1: Operating characteristics of the 775 laser line and relevant safety parameters.

Quantity	Symbol	Value
Beam radius	r	0.5 mm
Pulse width (FWHM)	τ	1.3 ns
Pulse repetition frequency	f	40 MHz
Pulse energy	E_{pulse}	31 nJ
Average power	P_{avg}	1.25 W
Thermal correction time	T_{min}	18 µs
Ca	C_a	1.41
Cc	C_c	1
Ce	C_e	1

Rule 1: The dose of a single pulse must not exceed the single-pulse MPE. The pulse dose H_{pulse} of the 775 nm laser at full power is

$$H_{pulse} = \frac{E_{pulse}}{2\pi r^2} \approx 39\,\mathrm{mJ/m^2}, \tag{D.1}$$

whereas the MPE equals

$$H_{pulse}^{MPE} = 5 \times 10^{-3} C_a C_e = 7.1\,\mathrm{mJ/m^2}. \tag{D.2}$$

This formula is found in table 2.2 of the regulations.

Rule 2: The dose of a single pulse may not exceed the thermally-corrected MPE. This weighs the pulse MPE with the amount of pulses in an interval T_{min}. The number of pulses in such an interval is $n = f \cdot T_{min}$, so

$$H_{thermal}^{MPE} = n^{-1/4} H_{pulse}^{MPE} = 1.3\,\mathrm{mJ/m^2}. \tag{D.3}$$

Rule 2 is therefore more strict than the rule 1. For safe operation, the laser must be ran at a power below 3.3% ($= H_{thermal}^{MPE}/H_{pulse}$).

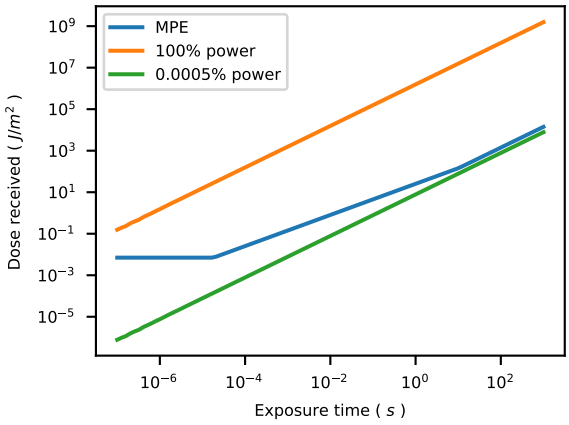

Figure D.1: Maximum permissible and actual exposure to the collimated STED beam as a function of exposure time.

Rule 3: The cumulative dose for a group of pulses in an interval of time t must not exceed the MPE for a single pulse of that time. Taking the necessary values from tables 2.2 and 2.3, the cumulative MPE is defined as

$$H_{tot}^{MPE}(t) = \begin{cases} 5 \times 10^{-3}\, C_a C_e & t < 18\,\mu\text{s}, \\ 18 t^{0.75}\, C_a C_e & 18\,\mu\text{s} < t < 10\,\text{s}, \\ 10 t\, C_a C_c & t > 10\,\text{s}. \end{cases} \tag{D.4}$$

The actual dose, on the other hand, is

$$H_{tot}(t) = \lfloor ft \rfloor H_{pulse}, \tag{D.5}$$

where $\lfloor \cdot \rfloor$ is the flooring function. This function is plotted in Figure D.1, from which it can be seen that the laser is only safe to use at 0.0005% capacity. Since the minimum laser power offered by the software is .05%, OD2 goggles should be worn to guarantee safe operation of the 775 nm laser.

E

Supplemental figures

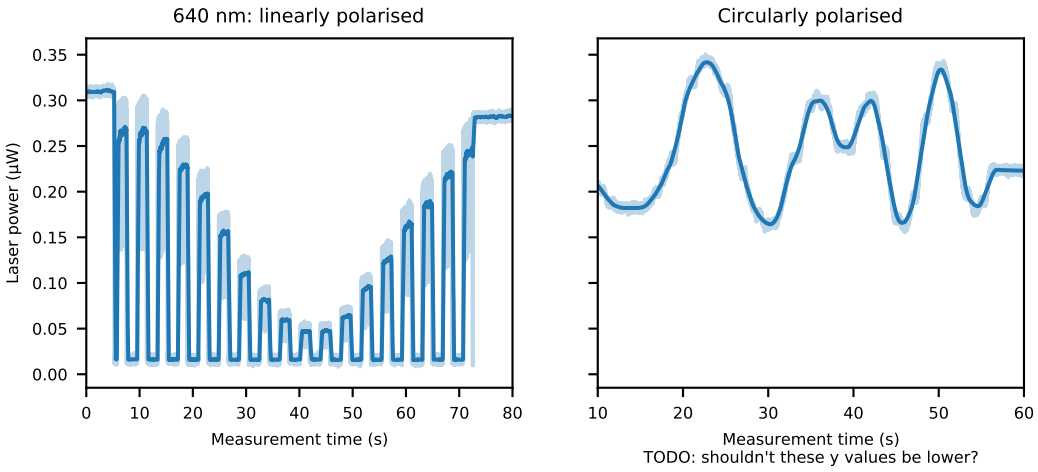

Figure E.1: Polarisation characteristics at the sample plane of the 640 laser. **Left:** power transmitted through a stationary polariser aligned to maximise transmission of the 640 laser set to an polarisation of 0° (vertical in the sample plane), while the laser beam rotates. **Right:** power transmitted through a manually rotating polariser, while the beam is set to circular polarisation.

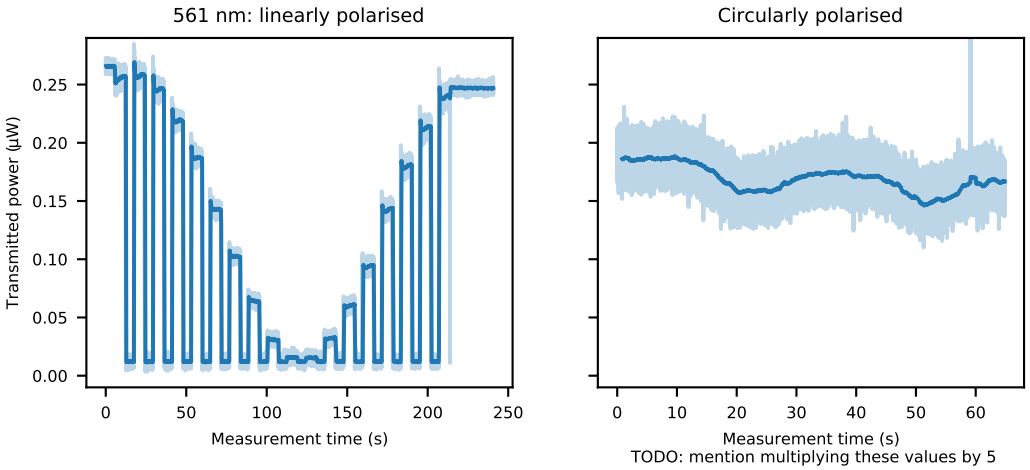

Figure E.2: Polarisation characteristics at the sample plane of the 561 laser. Left and right panes are the same as Figure E.1. (As the data on the left was acquired at 50% laser power to increase the signal at minimum transmission, but the data on the right was acquired at 10% laser power for safety reasons, the data on the right has been multiplied by a factor of 5 to allow comparison between the two figures. This also increased the noise.)

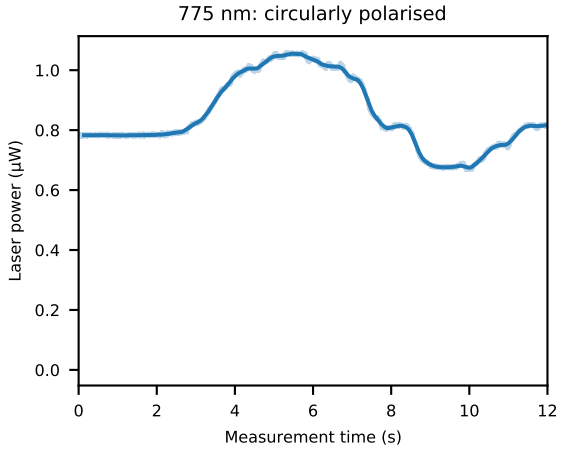

Figure E.3: Polarisation characteristics at the sample plane of the depletion beam, without pSTED optics. As its polarisation state cannot be manipulated through the software, only circular polarisation is characterised by manually rotating a polariser at the sample plane and measuring the transmitted power.

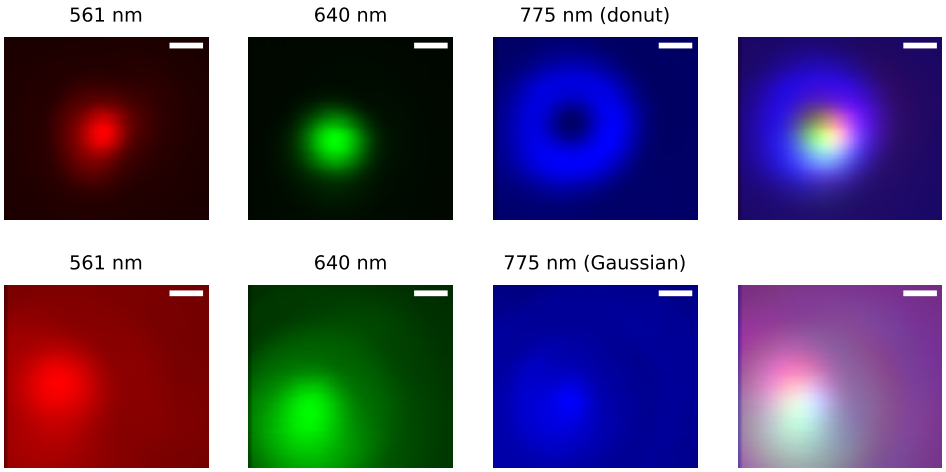

Figure E.4: Point spread functions of the different lasers at different SLM configurations, by measuring the reflection from 100 nm wide gold beads. Scale bars 200 nm. (show better data from 26 march)

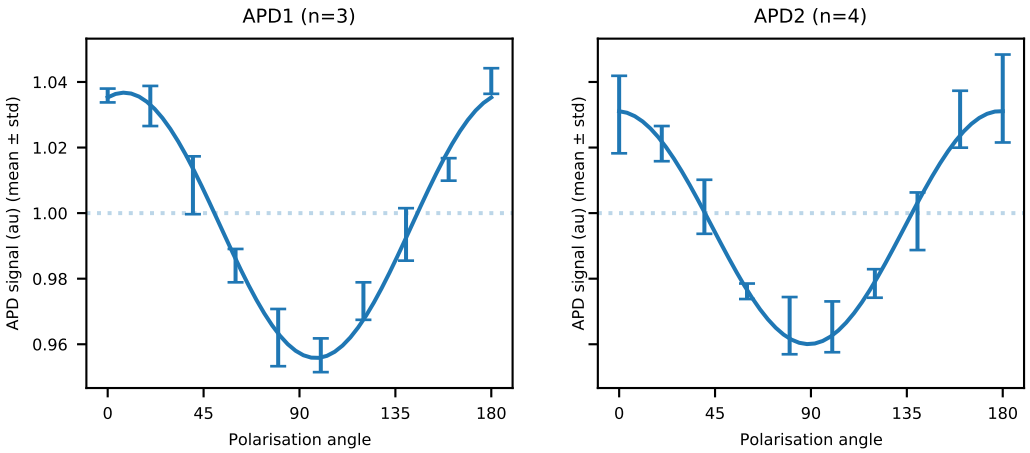

Figure E.5: Dependence of the signal from APD1 on the angle of polarisation of incoming light.

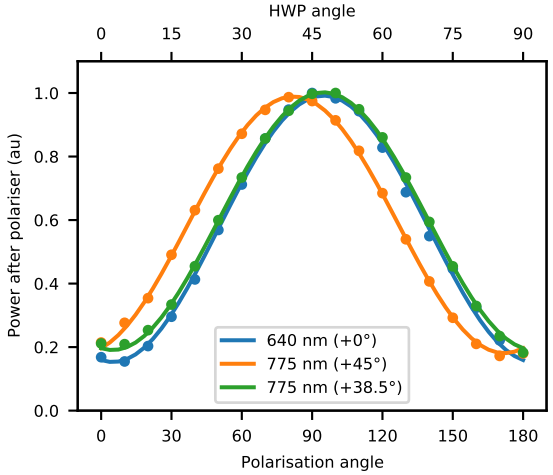

Figure E.6: The rotating HWP I put in the beamline controls the depletion beam polarisation. With an offset of 38.4°, the depletion beam is parallel to the 640 laser (set to vertical linear polarisation).